Dalton Transactions

PAPER

View Article Online
View Journal | View Issue

Check for updates

Cite this: *Dalton Trans.*, 2026, **55**, 5769

Nitrite binding modes in ferric heme proteins probed by HYSCORE spectroscopy

Ilenia Serra, †[a,b] Daniel Schmidt, ‡[c] Paul G. Furtmüller, [c] Pablo J. González, [d] Christian Obinger, [c] Sabine Van Doorslaer *[a] and Inés García-Rubio *[b,e]

Nitrite plays a fundamental role in the environmental nitrogen cycle and various biochemical reactions. Heme proteins such as globins and peroxidases, often participate in nitrite-mediated pathways, sparking interest in the coordination geometry of nitrite to the heme iron. In most cases, nitrite binds the ferric heme iron *via* the nitrogen atom (N-nitro mode), while for myoglobin and hemoglobin a less common *O*-nitrito ligation through one oxygen atom was reported. Our previous study on nitrite binding to the heme-containing enzyme chlorite dismutase (Cld) using continuous-wave electron paramagnetic resonance and crystal-field theory, supported by molecular dynamics simulations, suggested the coexistence of both *O*-nitrito and *N*-nitro ligation modes. Here, we present an in-depth hyperfine sublevel correlation (HYSCORE) analysis of NO_2-ligated ferric horse heart myoglobin, a Clade-II Cld from *Cyanothece* sp. PCC7425 and a Clade-I Cld from *Magnetospirillum* sp. ^{15}N-labelled nitrite was used to discriminate the signals ascribed to the nitrogen nucleus of nitrite from the endogenous N nuclei. The *O*-nitrito and *N*-nitro modes can be distinguished based on the nitrite nitrogen hyperfine coupling. Moreover, we describe a distinct HYSCORE spectral fingerprint for the *O*-nitrito binding mode which can be used as direct evidence of the ligation mode without further detailed analysis. Together, these results provide a generally applicable EPR/HYSCORE-based tool for (bio)inorganic nitrite coordination chemistry of heme systems, enabling more reliable interpretation of nitrite reactivity and mechanism in heme-based catalysts and nitrite-processing enzymes.

Received 22nd January 2026,
Accepted 16th March 2026

DOI: 10.1039/d6dt00171h

rsc.li/dalton

Open Access Article. Published on 18 March 2026. Downloaded on 5/4/2026 10:46:35 AM.
This article is licensed under a Creative Commons Attribution 3.0 Unported Licence.

Introduction

Nitrite (NO_2^-) is known to play a vital role in the environmental nitrogen cycle and in different biochemical pathways, including important signaling pathways.[1–3] Moreover, anthropogenic use of nitrite strongly impacts our daily life. Indeed, sodium nitrite (E249) and potassium nitrite (E250) are authorized and abundantly used as food additives, *e.g.*, for curing meat, which has raised some public concern as this use was suggested to lead to a higher incidence of cancer.[1] Nitrite is also therapeutically used, *e.g.*, as an antidote for cyanide poisoning.[4] In general, Nature's mechanistic strategies to form, reduce or oxidize nitrite are very diverse and still not fully understood, as reviewed in the article from Maia and Moura.[1]

Interestingly, many of the biological nitrite-mediated reactions involve heme proteins, such as globins and peroxidases.[1–3,5] In the early 2000 a previously unknown nitrite reductase (NiR) activity of deoxyhemoglobin was described for the first time.[6] This finding, among others, redefined the role of NO_2^- as an active player in several mammalian biological functions, with potential implications in dioxygen sensing, signaling pathways and as an O_2-independent reservoir of nitric oxide (NO). In addition to hemoglobin, the NiR activity was later demonstrated for other proteins in mammalian cells, including myoglobin (Mb),[7] endothelial alpha globin[8] and xanthine oxidase.[9] The relevance of nitrite in the medical field was further highlighted by studies on its interaction with myeloperoxidase and eosinophil peroxidase, the most abundant heme peroxidases in the leukocytes.[10,11] In addition to its importance in the physiology of mammals, nitrite plays a fundamental role

[a]*TSM² Group, Department of Chemistry, University of Antwerp, 2610 Antwerp, Belgium. E-mail: sabine.vandoorslaer@uantwerpen.be*
[b]*Department of Condensed Matter Physics, Faculty of Sciences, University of Zaragoza, 50009 Zaragoza, Spain. E-mail: inesgr@unizar.es*
[c]*Department of Natural Sciences and Sustainable Resources, Institute of Biochemistry, BOKU University, A-1190 Vienna, Austria*
[d]*Departamento de Física, Facultad de Bioquímica y Ciencias Biológicas, Universidad Nacional del Litoral, CP S3000ZAA Santa Fe, Argentina*
[e]*Instituto de Nanociencia y Materiales de Aragón, CSIC-Universidad de Zaragoza, 50009 Zaragoza, Spain*
†Present address: European Molecular Biology Laboratory (EMBL), Hamburg Outstation c/o DESY, Notkestrasse 85, 22607 Hamburg, Germany.
‡Present address: Institute of Medical Virology, University of Zurich (UZH), Zurich, Switzerland.

Open Access Article. Published on 18 March 2026. Downloaded on 5/4/2026 10:46:35 AM.
This article is licensed under a Creative Commons Attribution 3.0 Unported Licence.

in the environmental nitrogen cycle, being the substrate of bacterial NiRs, which are copper or heme-containing enzymes that reduce NO_2^- to ammonia in a six-electron transfer process.[12,13] Furthermore, a unique disproportionation of nitrite to NO and nitrate (NO_3^-) was described for nitrophorins (NPs), which are heme enzymes found in the saliva of the blood feeding insect *Rhodnius prolixus*.[14–16] Interestingly, GLB-33, the largest known globin of the model system *Caenorhabditis elegans* consisting of a globin domain and a 7 α-helices transmembrane domain, possesses *in vitro* an unusually high NiR activity.[17]

Because of the implication of a large variety of heme proteins in nitrite biochemistry, the coordination chemistry of NO_2^- in different heme-containing systems has been subject of numerous studies which aimed at elucidating the mode of binding of this anion to the heme iron and thus gaining mechanistic insights.[18–21] While in many cases nitrite was found to bind to the ferric heme iron in the so-called *N*-nitro mode[18] (Fig. 1A), the crystal structures of the nitrite-bound ferric myoglobin and hemoglobin show a less common *O*-nitrito ligation[19,20] (Fig. 1B). A site-directed mutagenesis approach combined with a structural and spectroscopic analysis revealed that in myoglobin the distal E7His is responsible for the *O*-ligation mode[21] and suggested a possible analogue role of the conserved distal histidine in human hemoglobin. While X-ray crystallography gives direct proof of the nitrite ligation mode in the ferric heme-protein case, this time-consuming technique relies on the success of the crystal growth. Moreover, both theoretical and experimental evidence indicates that the crystal structure may not always reflect the situation in solution, since the computed energy difference between the two binding modes is predicted to be very small for certain heme systems.[19,20,22–24] Hence, X-ray diffraction (XRD) results are often complemented with (a combination of) optical spectroscopies,[23,25,26] electron paramagnetic resonance (EPR)[22,25,27,28] and quantum-chemical computations[24,26] to elucidate the binding mode, but each technique comes with its own limitations.

In literature there is controversy about the interpretation of the continuous-wave (CW) EPR data of ferric nitrite-heme complexes in terms of the nitrite-ligation mode. Some studies relate nitrite binding to the appearance of the EPR signatures of low-spin (LS) ferric heme complexes, although they disagree on which LS species relates to which binding mode.[22,27,29] Other literature sources claim that the *O*-nitrito mode cannot be associated with the observation of an LS state with EPR, but is instead a high-spin (HS) ferric heme complex[28] or even an EPR-silent species.[28,30] Furthermore, it has been observed that nitrite may also induce greening of some heme proteins caused by the reaction of a heme vinyl group and nitrite to form a nitrovinyl group.[31–33] Resonance Raman data suggest that Fe(III) spin-state changes from LS to HS may occur in the *O*-nitrito/2-nitrovinyl form of Mb and that this is associated with an increase in the bond length between the heme iron and the proximal His nitrogen.[26]

Chlorite dismutases are heme-containing bacterial oxidoreductases which decompose chlorite into chloride and molecular dioxygen, a reaction in which the distal catalytic arginine plays a key role.[34–36] According to the most recent classification, Clds are divided in two clades, namely Clade I (or "long Clds") comprising mostly pentameric representatives, and Clade II (or "short Clds") containing dimeric enzymes, such as *Cyanothece* sp. PCC7425 (*C*Cld).[37] In a recent study, we examined the ligation of nitrite to wild-type and variants of *C*Cld.[22] This study focused on the impact of the distal arginine on the binding of angulate ligands, such as nitrite and chlorite, by combining several experimental and theoretical methods. While X-ray crystallography revealed an *O*-nitrito binding mode (Fig. 1C), multiple LS species were observed in the CW-EPR spectra. We tentatively ascribed these species to a co-existence of the *N*-nitro and *O*-nitrito binding modes. However, although the interpretations were based on the comparative crystal-field analysis of the parameters for different heme proteins and were supported by molecular dynamics simulations on *C*Cld-NO_2^- complexes, the proof of the heterogeneous binding modes remained indirect.

The ^{14}N hyperfine couplings of endogenous and exogenous N-ligands of the heme iron are directly related to the electronic

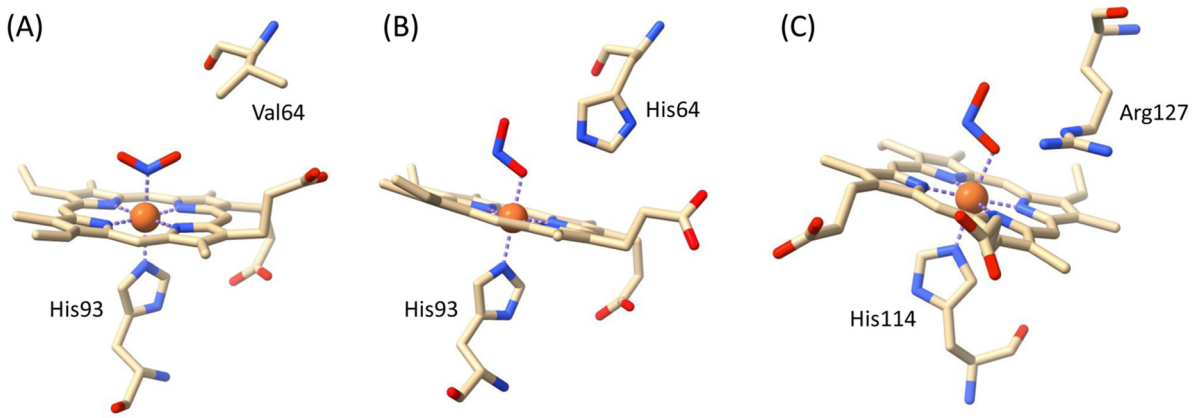

Fig. 1 Representation of (A) the *N*-nitro ligation mode in the H64 V variant of sperm whale Mb (PDB ID: 6CF0), (B and C) the *O*-nitrito ligation modes in wild-type horse heart Mb (PDB ID: 2FRF) (B) and wild-type chlorite dismutase from *Cyanothece* sp. PCC7425 (PDB ID: 7OU5) (C).

This journal is © The Royal Society of Chemistry 2026

Open Access Article. Published on 18 March 2026. Downloaded on 5/4/2026 10:46:35 AM. This article is licensed under a Creative Commons Attribution 3.0 Unported Licence.

and geometric structure, and thus to the ligand binding modes. Hyperfine sublevel correlation (HYSCORE) spectroscopy offers a powerful tool to determine these hyperfine interactions in paramagnetic systems[38–44] and can potentially probe the nitrite coordination geometry at ferric heme centers, which may then open further applications in (bio)inorganic studies of nitrite activation, reduction and disproportionation across different heme protein and their synthetic mimics. To test this hypothesis and to clarify some of the existing ambiguities in the assignments of EPR spectra of nitrite complexes of heme proteins, we performed a detailed HYSCORE analysis of NO_2^--ligated ferric horse heart Mb, Clade-II *C*Cld and the Clade-I Cld from *Magnetospirillum* sp. (*Ma*Cld). In order to distinguish the nitrite-specific HYSCORE signals from the ones of the numerous nitrogen nuclei in the heme iron proximity (*i.e.*, from the pyrrole and the proximal histidine), we used ^{15}N-isotope labeling. In addition to resolving the specific case of Clds, the study reveals HYSCORE fingerprint signals that can be transferred to other ferric nitrite–heme systems where CW-EPR and other spectroscopic signatures are ambiguous.

Experimental

Standard and ^{15}N-labelled sodium nitrite ($NaNO_2$) were purchased from Sigma Aldrich. Tris-HCl pH 7.0 was prepared at a concentration of 100 mM. The "temperature independent (TIP)" buffer was prepared by mixing 45% HEPES pH 7.0 and 55% sodium phosphate buffer pH 7.0 in order to minimize the variation in pH upon freezing.[45] Both buffers were filtered and degassed prior to use. Myoglobin (Mb) from horse heart muscle (95–100% pure, essentially salt-free, lyophilized powder) was also purchased from Sigma-Aldrich and used without further purification. Wild-type chlorite dismutase from *Cyanothece* sp. PCC7425 was recombinantly produced in *E. coli* BL21 Gold (DE3) cells (Agilent) and purified as previously described.[46] Wild-type Cld from *Magnetospirillum* sp. was purified up to electrophoretic grade from *Mangetospirillum* sp. cells as described before.[47] Myoglobin samples were prepared as follows: sodium nitrite (either standard or ^{15}N-labelled) was dissolved in 100 mM Tris-HCl pH 7 to a final concentration of 1 M. Then, 50 μL of this solution were mixed with 50 μL of glycerol in order to obtain a solution containing 50 mM Tris-HCl, 500 mM $NaNO_2$ and 50% (v/v) glycerol. The solutions of $NaNO_2$ were freshly made before each sample preparation. Next, ~2 mg of lyophilized Mb were dissolved in the buffered nitrite solution to reach a final protein concentration of ~1 mM. Samples of *Ma*Cld were prepared by adding glycerol to the protein solution in 50 mM Tris-HCl buffer already containing $NaNO_2$. Similarly, samples of wild-type *C*Cld and mutant R127A were prepared by mixing 50 μL of glycerol and 50 μL of a solution containing 100 mM TIP buffer pH 7.0, 1 M $NaNO_2$ and 2 mM *C*Cld in order to obtain the same final concentrations and nitrite-to-protein ratio as in the Mb samples. TIP buffer was used in the case of *C*Cld following the strong pH dependency of the heme cofactor spin state that we observed earlier.[46]

Both CW and pulsed EPR measurements were performed on a Bruker ELEXSYS E580 X-band spectrometer equipped with an Oxford CF935 continuous-flow cryostat and either a Bruker ER4118 SPT-N1 resonator or a Dielectric Ring Resonator ER4118X-MD5, both operating at a MW frequency of ~9.7 GHz. CW-EPR spectra were recorded at 10 K under non-saturating conditions, with modulation amplitude of 1 mT and a modulation frequency of 100 kHz. For field-swept ESE-detected EPR measurements, a Hahn echo sequence $\pi/2$–τ–π–τ–echo with 2-step phase cycling was used. $\pi/2$ (π) pulse length was 16 (32) ns. Other settings are mentioned in the figure legends. The HYSCORE experiments were performed at 10 K using the sequence $\pi/2$–τ–$\pi/2$–t_1-π–t_2–$\pi/2$–τ–echo with $\pi/2$ (π) pulse length of 16 (32) ns. In the case of *Ma*Cld, the initial t_1 and t_2 were 96 ns and they were increased in steps of 16 ns. For wild-type *C*Cld and mutant R127A, t_1 and t_2 varied from 112 to 4284 ns in steps of 28 ns or 32 ns, respectively. A 4-step phase cycling was used in all cases.[48] For all pulsed experiments, the shot repetition time was of 1 ms. Simulations of CW and pulsed EPR spectra were performed with the EasySpin software implemented in MATLAB (v. 6.0.0-dev.41).[49]

Results and discussion

CW-EPR signatures of the low-spin nitrite-ferric heme complexes under study

The CW-EPR and electron–spin-echo (ESE)-detected EPR spectra of NO_2^--ligated forms of ferric wild-type Mb and *C*Cld are depicted in Fig. S1 and S2 of the SI and show typical EPR features of LS heme complexes, in line with earlier results.[22,50] Fig. S3 depicts the EPR spectrum of the ferric *Ma*Cld-NO_2^- complex, with Table 1 showing the related principal *g* values in comparison with literature data of other nitrite-ligated heme systems and known information from other techniques (if

Table 1 Principal *g* values of the nitrite complexes of the ferric heme proteins under study in comparison with reported EPR data and knowledge on the nitrite ligation binding mode from other techniques

Protein	LS#	g_x	g_y	g_z	Ref.	Ligation mode
*C*Cld wt	LS1	1.64	2.24	2.87	22	O (XRD)[22]
	LS2	1.62	2.40	2.73		
	LS3	1.62	2.42	2.69		
*C*Cld R127A	HS	6.00	5.61	1.99		O (XRD)[22]
	LS1	1.58	2.23	2.88	22	
	LS2*	1.60	2.38	2.78		
*Ma*Cld	LS4	1.555	2.195	2.958	This work	
Mb	LS5	1.57	2.20	2.95	22	O (XRD),[19] RR[26]
*Ao*Cld		1.55	2.18	2.93	51	
NP4		1.51	2.41	2.72	16	N (XRD)[16]
Cytc′L16G		1.56	2.36	2.84	23	N (XRD), N (FTIR)[23]

O = *O*-nitrito mode, N = *N*-nitro mode, XRD = X-ray diffraction, FTIR = Fourier Transform infrared spectroscopy, RR = Resonance Raman spectroscopy, wt = wild-type, *Ao*Cld = Clade-I chlorite dismutase from *A. orizae*, NP4 = Nitrophorin 4 from *Rhodnius prolixus*, CytcL16G = L16G mutant from *Alcaligenes xylosoxidans* cytochrome c′. At pH 7.0, the ratio of LS1 : LS2 : LS3 in wt *C*Cld is 58 : 29 : 13, while the ratio HS : LS1:LS2 in *C*Cld R127A is 9 : 35 : 56.[22.]

Open Access Article. Published on 18 March 2026. Downloaded on 5/4/2026 10:46:35 AM.
This article is licensed under a Creative Commons Attribution 3.0 Unported Licence.

available). While three low-spin forms are detected for the nitrite complex of *C*Cld (LS1–3), only one is found for *Ma*Cld (LS4) with principal *g* values very close to those of the *O*-nitrito bound nitrite complex of Mb (LS5) and of *Ao*Cld (Table 1). Our previous crystal-field analysis of the principal *g* values of LS1–3 of *C*Cld-nitrite[22] suggested the presence of both *O*-nitrito bound (LS1) and *N*-nitro bound (LS2–3) nitrite complexes for *C*Cld, but the species identification was far less clear-cut than in the LS4 case. While molecular dynamics simulations supported the potential co-existence of the two binding modes, only the *O*-nitrito form was observed for *C*Cld using X-ray crystallography.[22] To strengthen the interpretation of the EPR spectra of the nitrite-ligated Cld proteins, $^{14}N/^{15}N$ HYSCORE is performed, with the analysis of the Mb-nitrite complex used as a methodological benchmark.

HYSCORE analysis of the nitrite-binding mode in ferric myoglobin (LS5)

Using density functional theory (DFT) computational methods, Sundararajan and Neese predicted that the hyperfine coupling to the ^{14}N nucleus of the nitrite ligand of nitrite-ligated Mb will differ of an order of magnitude depending on whether the ligand is *O*-nitrito bound or *N*-nitrito bond, with the predicted values falling within the typical frequency range probed by hyperfine spectroscopy, such as HYSCORE.[24] Given that nitrite binding to the ferric (wild-type) myoglobin is known to occur through the uncommon *O*-nitrito mode,[19,20] this system is used as a model for this nitrite-binding mode in HYSCORE spectra. In order to distinguish the HYSCORE signals from the multiple nitrogen nuclei in the heme iron proximity from those of nitrite, ^{15}N-labelled nitrite was used in addition to standard (^{14}N-rich) nitrite. The isotope exchange has no significant influence on the position or linewidth of the spectral features of the CW-EPR spectrum (see Fig. S1A), indicating that the hyperfine coupling to the nitrite N nucleus is small. In contrast, the corresponding ESE-detected EPR spectra (Fig. S1B) are affected by the isotope exchange due to nuclear modulation effects.[52] This is a first indication that the interactions between the unpaired electron and the nitrite nucleus can be detected by hyperfine spectroscopy.

Fig. 2 shows the superimposed X-band HYSCORE spectra of the $^{14}NO_2^-$- and $^{15}NO_2^-$-bound myoglobin, in black and magenta respectively, taken at the observer position corresponding to g_z. While the cross peaks in the (−,+) quadrant can be easily superimposed, considerable differences are observed in the (+,+) quadrant. Two well-resolved cross peaks centered around the Larmor frequency of ^{15}N are found for the $^{15}NO_2^-$ case (Fig. 2, Fig. 3B(left)), revealing the weak coupling to the nitrogen of the isotope-labelled nitrite in line with what is expected for the *O*-nitrito binding mode. In the (−,+) quadrant the characteristic spectral shape of the HYSCORE spectra of a ferric heme system can be easily recognized with prominent double-quantum (DQ) cross peaks ascribed to two pairs of pyrrole nitrogen nuclei and the single-quantum (SQ) and DQ cross peaks of the strongly coupled ^{14}N from the proximal histidine (His93) (Fig. 2 and Fig. S4A–C).[40–43,53] In

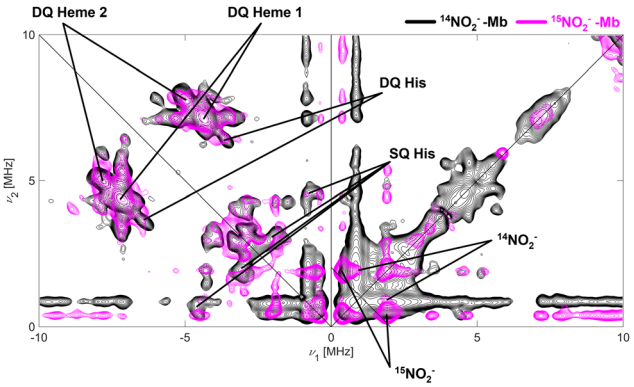

Fig. 2 X-band HYSCORE spectra of 1 mM ferric horse heart myoglobin in presence of 500 mM of either $^{14}NO_2^-$ (black) or $^{15}NO_2^-$ (magenta), taken at the observer position corresponding to $g = g_z$. The figure represents the sum of spectra taken with τ = 96, 176 and 208 ns, normalized to the noise level. The antidiagonal drawn in the (+,+) quadrant crosses the main diagonal at the Larmor frequency of ^{15}N at the selected magnetic field position (234.7 mT).

the high-frequency region of the (−,+) quadrant, as typically reported in other LS ferric heme centers, combination peaks of the ^{14}N DQ nuclear frequencies of two heme nuclei and of the heme and His DQ frequencies are visible. These peaks are clearly resolved at both the observer positions $g = g_z$ and $g = g_x$, the latter depicted in Fig. S4D and can be used to experimentally determine the relative sign of the hyperfine couplings.[41] Note that at the observer positions corresponding to $g = g_y$ and $g = g_x$, the spectral features in both (−,+) and (+,+) quadrants are almost completely superimposable (Fig. S5A and B). All spectral simulations are depicted in Fig. S6 and S7, while the final simulation parameters obtained for the porphyrin, His ^{14}N and $^{14}N/^{15}N$ nitrite, are presented in Table 2 in comparison with values reported in literature for other globin-ligand complexes.[54,55] Note that the absolute sign of the parameters cannot be determined experimentally, but it was taken based on the theoretical predictions and comparison with similar systems.[24,41]

As it can be seen from Table 2, the A_{zz} and Q_{zz} values which describe the coupling with the heme nitrogen nuclei are in line, at least in absolute value, with the ones previously reported for myoglobin in complex with other ligands, such as imidazole or azide. However, because the full characterization of the coupling tensor is missing for the reported myoglobin complexes, the comparison has to be considered with appropriate caution. The features ascribed to the ^{14}N nucleus from the coordinating proximal histidine can be simulated with similar $|A_{zz}|$ as the myoglobin–imidazole complexes,[54,55] but differ from the values reported for a myoglobin–azide complex.[57] This may be because the coordination of the proximal histidine is affected by the nature of the sixth ligand; however, the values reported for the myoglobin–azide complex need to be taken with caution since they were determined by 3-pulse ESEEM only, which are normally less accurate than HYSCORE.[59] Furthermore, the full ^{14}N $\boldsymbol{A}$ and $\boldsymbol{Q}$ tensors of the

 This journal is © The Royal Society of Chemistry 2026

Open Access Article. Published on 18 March 2026. Downloaded on 5/4/2026 10:46:35 AM.
This article is licensed under a Creative Commons Attribution 3.0 Unported Licence.

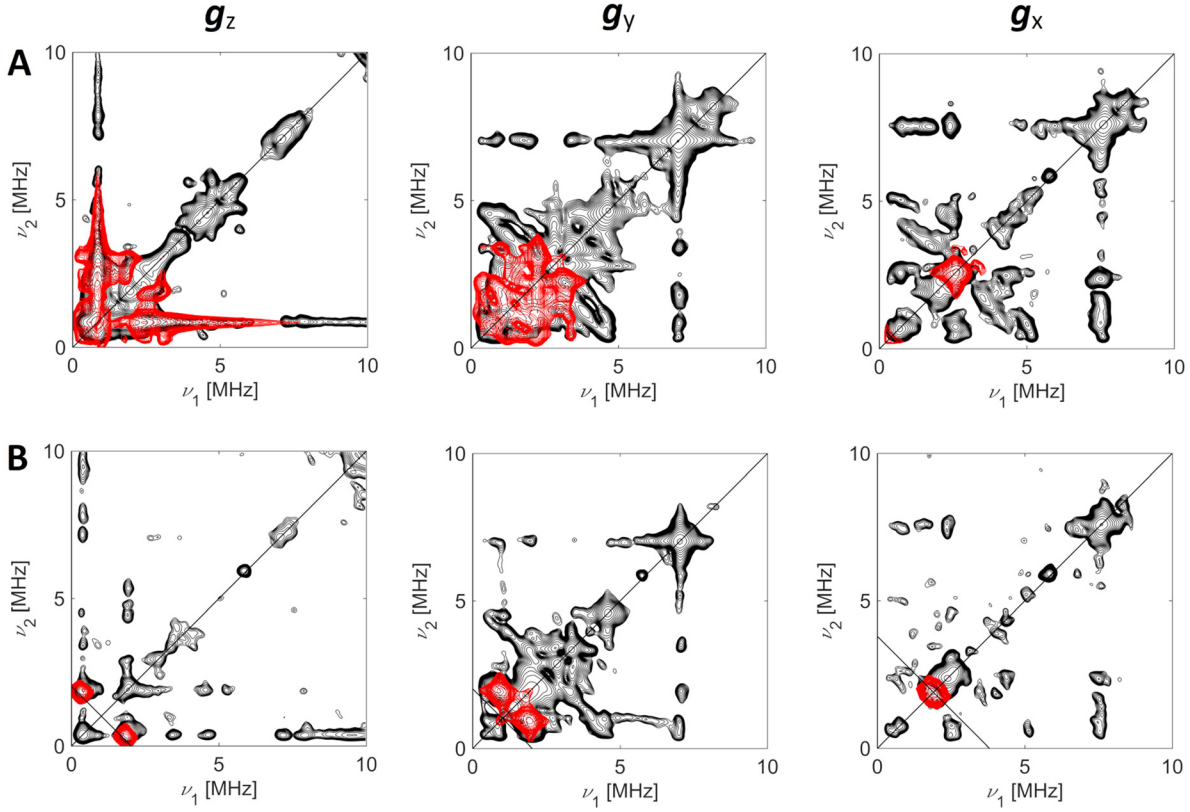

Fig. 3 Experimental (black) and simulated (red) X-band HYSCORE spectra ((+,+)-quadrant only) of 1 mM ferric horse heart myoglobin in presence of 500 mM of $^{14}NO_2^-$ (A), or $^{15}NO_2^-$ (B), recorded at the observer positions corresponding to $g = g_z$, $g = g_y$, and $g = g_x$, as indicated above the panels. The figures represent the sum of spectra taken with τ = 96, 176 and 208 ns, normalized to the noise level. The simulation includes exclusively one weakly-coupled nitrogen nucleus from nitrite.

Table 2 Principal hyperfine (A) and quadrupole (Q) values (in MHz) of the nitrogen nuclei in nitrite-bound ferric myoglobin in comparison with literature data for other myoglobin complexes and for ferric cytoglobin

	A_{zz}	A_{yy}	A_{xx}	Q_{zz}	Q_{yy}	Q_{xx}	α, β, γ (°)	Ref.
hhMb-NO_2^-								
Heme 1	−5.64	−4.70	−4.70	−0.45	−0.40	0.85	70, 0, 0	
Heme 2	−6.37	−5.00	−5.00	−0.45	−0.40	0.85	−20, 0, 0	
His	−4.95	−6.15	−5.50	−0.90	0.10	0.80	0, 0, 0	This work
^{14}N-NO_2^-	−1.35	−0.57	−0.11	−0.95	0.05	0.90	90, 20, 90	
^{15}N-NO_2^-	1.90	0.80	0.15	—	—	—	90, 20, 90	
hhMb-Im[a]								
Heme 1	5.60[b]	n.d.	n.d.	0.50[b]	n.d.	n.d.	n.d.	
Heme 2	6.20[b]	n.d.	n.d.	0.50[b]	n.d.	n.d.	n.d.	54
His/Im	5.00[b]	n.d.	n.d.	0.85 [b]	n.d.	n.d.	n.d.	
swMb-Im[a]								
Heme 1	5.80[b]	n.d.	n.d.	0.46[b]	n.d.	n.d.	n.d.	
Heme 2	6.40[b]	n.d.	n.d.	0.53[b]	n.d.	n.d.	n.d.	55
His/Im	5.70[b]	n.d.	n.d.	n.d.	n.d.	n.d.	n.d.	
hhMb-N_3^-[a]								
Heme 1	−5.64	n.d.	n.d.	n.d.	n.d.	−0.55	n.d.	56
Heme 2	−6.14	n.d.	n.d.	n.d.	n.d.	−0.62	n.d.	
His	−3.00	−4.60	−4.60	−0.80	0.36	0.44	0, 10, 0	57
CYGB								
Heme	−5.45	−4.10	−4.00	−0.42	0.92	−0.50	0, 0, 0	58
His	−5.00	−4.70	−5.90	−0.90	0.56	0.34	0, 0, 0	

α, β, and γ are the Euler angles (in degrees) applied to both the $\boldsymbol{A}$ and $\boldsymbol{Q}$ tensors frames for each nucleus. Errors on A values: ±0.05 MHz; errors on Q values: ±0.05 MHz; errors on Euler angles: ±10 deg. hhMb = horse heart myoglobin, swMb = sperm whale myoglobin, CYGB = cytoglobin, Im = imidazole, N_3 = azide, n.d. = not determined. [a] The errors on these values are reported on original papers. [b] Originally reported as absolute values.

Open Access Article. Published on 18 March 2026. Downloaded on 5/4/2026 10:46:35 AM. This article is licensed under a Creative Commons Attribution 3.0 Unported Licence.

coordinating distal and proximal His in cytoglobin are in line with the couplings observed here for hhMb-NO_2^-, further corroborating our assignment.[58]

The contribution from a weakly-coupled nitrogen atom from nitrite was simulated independently using the procedure outlined in the SI (values in Table 2) and the obtained simulated spectra are shown in Fig. 3. Note that although the ridges appear in the low-frequency range, the position and lineshape of ^{14}N and ^{15}N signals scale according to their nuclear magnetic moment, excluding relevant distortions caused by base-line subtractions in the time domain. A satisfactory simulation is obtained with $|e^2Qq/h|$ = 1.9 MHz and an almost completely axial $\boldsymbol{Q}$ tensor for the nitrite ^{14}N nucleus. The value is unexpectedly low in comparison to the value obtained from nuclear quadrupole resonance (NQR) spectroscopy for $NaNO_2$ ($|e^2Qq/h|$ values in range of 5.5–5.79 MHz are reported[60,61]). The z-axis of the $\boldsymbol{Q}$ tensor appears to be tilted by about ~20° with respect to the $\boldsymbol{g}_z$-axis, which is in turn expected to be collinear with the Fe–O bond. This is consistent with the angulate structure of the nitrite molecule, which possesses an O–N–O bond angle of ~113° and with an O–Fe–N angle of ~26° estimated from the PDB structure of the nitrite-bound myoglobin (PDB ID: 2FRF, Fig. 1B). Sundararajan and Neese theoretically considered two possible arrangements of the *O*-nitrito bound ligand in the heme pocket.[24] One is the $-ONO_T$ configuration with the nitrite in the orientation as found by XRD (Fig. 1B). In the second form, $-ONO_C$, the nitrite molecule is more bent towards the heme pocket and the outer oxygen is much closer to the heme plane. The predicted A_{zz} values for the ^{14}N of nitrite were −1.2 MHz and −3.3 MHz for $-ONO_T$ and $-ONO_C$, respectively. Comparison with the experimental value (Table 2) shows that the $-ONO_T$ data match very well with our observations and further corroborates the match between the XRD and EPR results. Furthermore, the isotropic hyperfine values, *i.e.*, the average of the principal hyperfine values, of the heme and His93 nitrogen nuclei were also computed and found to be very similar and approximately 7 MHz for both models.[24] This is matching the trend and order of magnitude found experimentally (heme: −5.0 and −5.5 MHz; His93: −5.5 MHz). To the best of our knowledge, the only other pulsed EPR investigation of nitrite-ligated myoglobin was performed by Bawn and McMillan (non-peer reviewed report[50]). Upon addition of nitrite to ferric Mb, they observed the formation of a LS complex with g values comparable to the ones we reported above (LS5, Table 1), but the nitrite ^{14}N hyperfine and quadrupole parameters that they obtained from the simulation of 3-pulse ESEEM spectra differ from the ones we reported here from HYSCORE data (Table 2). It has to be noted that the simulations were performed only for the observer position $g = g_z$ and neither the Euler angles nor a figure depicting the simulations were presented. Moreover, the authors very briefly describe a matched HYSCORE spectrum by simply highlighting the presence of a weakly-coupled ^{14}N which they assign to nitrite, without further analysis.

HYSCORE fingerprint for *O*-nitrito binding in nitrite-bound ferric *Ma*Cld

The above HYSCORE analysis of the $^{14}NO_2^-$-bound myoglobin suggests that the appearance of the sharp, elongated ridges in the (+,+) quadrant of the HYSCORE spectrum at the magnetic field position corresponding to $g = g_z$ (Fig. 2 and 3A) may be used as a fingerprint for *O*-nitrito binding in other nitrite-binding heme proteins. In order to confirm this hypothesis, a similar approach is used for nitrite-bound ferric *Ma*Cld (LS4), a complex with very similar principal g values (and thus ligation mode) as nitrite-bound Mb (Table 1). The HYSCORE spectrum at this observer position indeed shows these characteristic features (Fig. S8), corroborating the potential of using this as a fingerprint for the *O*-nitrito binding mode.

The complex HYSCORE profile of nitrite-bound *C*Cld: *O*-nitrito *versus N*-nitro binding mode

As discussed in section 3.1, the EPR spectrum of nitrite-bound *C*Cld shows multiple LS species (LS1–3), with a less clear-cut identification of the ligation modes. Similar to what has been observed for myoglobin, the X-band CW-EPR measurements of wild-type *C*Cld bound to either ^{14}N or ^{15}N-labelled nitrite showed no significant differences (Fig. S2), indicating that for all three LS forms (LS1–3) the hyperfine couplings of the nitrite nitrogen nucleus is small compared to the typical line broadening for these systems. The interpretation of the HYSCORE spectra is hampered by the large spectral overlap of the EPR signals of LS1–3. Since all three values for g_x are very similar, only at the magnetic field range between the positions corresponding to g = 2.87 (g_z of LS1) and g = 2.74 (g_z of LS2) a single species (LS1) contributes. At all other magnetic-field positions, there is signal overlap of different species and hence multiple species contribute to the HYSCORE spectra for those observer positions. Therefore, we initially focused on the HYSCORE spectrum taken at the magnetic field position corresponding to $g = g_z$ of LS1, herein referred to as "g_z(1)", which only includes contributions of LS1 (Fig. 4). Again, the sharp ridges attributed to $^{14}NO_2^-$ in the *O*-nitrito mode are observed in the (+,+) quadrant, with its assignment confirmed by experiments performed with $^{15}NO_2^-$ (Fig. S9A). Therefore, the dominant component of the EPR spectrum of nitrite-bound *C*Cld, LS1, can be linked to the *O*-nitrito binding mode, as hypothesized by the crystal-field analysis of the g values and observed by XRD.[22]

In the HYSCORE spectrum depicted in Fig. 4, the DQ cross peaks typical of the heme nitrogen nuclei are visible, as well as the SQ transitions univocally attributed to the Fe-binding nitrogen of the proximal histidine (His114). The DQ cross peaks of the latter interaction are not clearly resolved at this magnetic field position, in contrast to the case of myoglobin (Fig. 2 and Fig. S4). Comparison of the HYSCORE spectra of the complexes of ferric *C*Cld with ^{14}N-labeled and ^{15}N-labeled nitrite taken at different observation positions (Fig. S9–S11) indicates that ^{15}N-related signals are present in the low-frequency area of the (+,+)-quadrant of all spectra. Given that LS1

 This journal is © The Royal Society of Chemistry 2026

Open Access Article. Published on 18 March 2026. Downloaded on 5/4/2026 10:46:35 AM.
This article is licensed under a Creative Commons Attribution 3.0 Unported Licence.

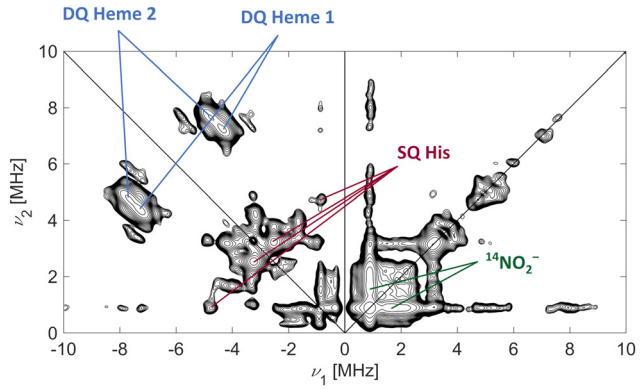

Fig. 4 X-band ^{14}N-HYSCORE spectrum of 1 mM wild-type *C*Cld in presence of 500 mM of $^{14}NO_2^-$, pH 7.0, taken at the observer position corresponding to $g_z(1)$ (243 mT). The figure represents the sum of spectra taken with two τ-values (176 and 208 ns), normalized to the noise level.

contributes to all observer positions, we attribute them to the coupling of the distal nitrite nitrogen nucleus of the *O*-nitrito ligated species LS1.

Interestingly, HYSCORE spectra in the region of magnetic field where LS2 and LS3 contribute show a pair of cross peaks which are absent in the $^{15}NO_2^-$-bound protein. The superimposed (−,+) HYSCORE quadrant of $^{15}NO_2$- and $^{14}NO_2$-bound *C*Cld for magnetic field settings corresponding to $g_y(1)$ and $g_y(2) \approx g_y(3)$ is shown in Fig. 5, where these specific peaks have been indicated by red arrows. These correlation peaks cannot be found in the $^{15}NO_2^-$-bound spectrum, even using a low contour cutoff level, and they lie close to the double quantum lines of the spectrum since the nuclear frequencies are spaced ~3.7–3.9 times the Larmor frequency of ^{14}N at the relative magnetic field positions. As they correspond to a coupling of about 9 MHz (A_{yy}), they do not match what is expected for signals of a weakly coupled ^{14}N nucleus. Moreover, since these peaks were not observed in the corresponding spectra of nitrite-ligated Mb and they do not correspond to combinations of other nuclear frequencies (see below), we assign them to DQ cross peaks of a strongly-coupled ^{14}N nucleus from a molecule of nitrite coordinating through the *N*-nitro mode. This substantiates the indication from the ligand-field analysis of the ***g*** tensors that LS2 and LS3 represent species with this form of ligation.[22]

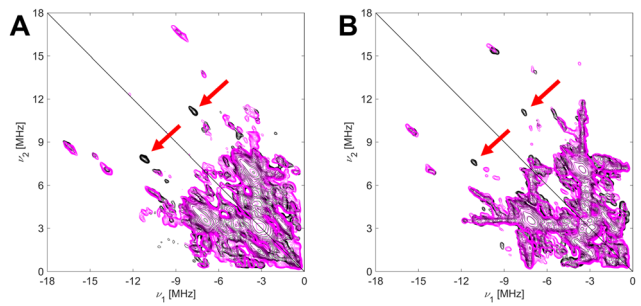

Fig. 5 X-band HYSCORE spectra ((−,+) quadrant) of 1 mM wild-type *C*Cld in presence of 500 mM of either $^{14}NO_2^-$ (black) or $^{15}NO_2^-$ (magenta), taken at the observer position corresponding to (A) $g = g_y(2) \approx g_y(3)$ (288.4 mT) and (B) $g = g_y(1)$ (310 mT). The spectra are the sum of spectra taken with τ = 176 and 208 ns, normalized to the noise level. The red arrows indicate the additional peaks exclusively observable in the $^{14}NO_2^-$ spectrum.

The simulations of the nitrite-bound *C*Cld HYSCORE spectra were performed with a similar approach as used for myoglobin in section 3.2. Initially, the observer positions corresponding to $g_z(1)$, $g_y(1)$ and g_x were considered and only the contributions for the heme and His114 ^{14}N were simulated. While at the $g_z(1)$ position a 4-spin system ($S = \frac{1}{2}$, 2 × heme N, 1 × His114 N) was sufficient to describe the "single species" spectrum and resulted in a rather satisfactory simulation (Fig. S12A), this was not the case for the intermediate positions, where HYSCORE signals stemming from LS1, LS2 and LS3 are simultaneously present (Fig. S12B and C). The corresponding spectra obtained with $^{15}NO_2^-$ have been simulated with the same parameters (Fig. S13). An additional weakly-coupled N from nitrite was simulated separately, using the same approach already described for the myoglobin case (Fig. S14).

Obtaining the full set of parameters of the strongly-coupled nitrite N nucleus for LS2 and LS3 is a hard task, since the peaks assigned to $^{14}NO_2$ in the *N*-nitro mode of ligation have only been detected in the central region of absorption spectrum. Fig. S15 shows a tentative simulation of the spectra taken at the magnetic field positions of $g_y(1)$ and $g = g_y(2) \approx g_y(3)$, which includes the contribution of the heme N nuclei and one additional strongly-coupled N nucleus. The hyperfine and nuclear quadrupole principal values used for the simulation need to be taken with caution, since the peaks (treated here as DQ) are visible only in a limited range of the magnetic field. In any case, a simulated spectrum without unrealistic extra peaks at all the magnetic field positions could be obtained with the parameters $A_{zz} = -16$ MHz, $A_{yy} = -9$ MHz and $A_{zz} = -7.7$ MHz; $Q_{zz} = 2$ MHz, $Q_{yy} = -1.5$ MHz and $Q_{zz} = -0.5$ MHz, taking the ***A*** and ***Q*** tensor frames collinear with the ***g*** tensor one. When a ^{15}N signal is simulated with the values used for ^{14}N multiplied times $\nu_{L(^{15}N)}/\nu_{L(^{14}N)}$ to obtain the corresponding hyperfine (Fig. S16), the features assigned to the DQ of $^{14}NO_2$ disappear, indicating that the peaks do not stem from combination frequencies and supporting the assignment to a strongly-coupled N from NO_2^-. Sundararajan and Neese predicted a value of −19 MHz for A_{zz} in the case of an *N*-nitro ligation mode.[24] Unfortunately, they did not report the other principal values. All the simulation values are reported in Table 3, in comparison with the hyperfine values previously found for ferric *Ma*Cld forming a LS complex with either imidazole or azide.[42]

In our previous work, we showed that the nitrite-bound form of a *C*Cld mutant in which the catalytic arginine was replaced by an alanine (R127A), displays both the LS1 species and an additional LS species with principal *g* values very similar to LS2–LS3. This species, that here we refer to as LS2*

Open Access Article. Published on 18 March 2026. Downloaded on 5/4/2026 10:46:35 AM.
This article is licensed under a Creative Commons Attribution 3.0 Unported Licence.

Table 3 Principal hyperfine (*A*) and quadrupole (*Q*) values (in MHz) of the nitrite-bound CCld in comparison with other LS complexes of MaCld with different axial ligands

	A_{zz}	A_{yy}	A_{xx}	Q_{zz}	Q_{yy}	Q_{xx}	α, β, γ (°)	Ref.
CCld-NO_2^- (LS1)								
Heme 1	−5.70	−5.10	−4.90	−0.30	−0.45	0.75	60, 0, 0	
Heme 2	−6.33	−5.95	−4.90	−0.30	−0.45	0.75	−30, 0, 0	
His	−5.65	−6.30	−6.45	−0.87	0.55	0.32	30, 0, 0	This work
^{14}N-NO_2^-	1.07	1.14	−0.14	−0.95	0.05	0.90	90, 20, 90	
^{15}N-NO_2^-	1.50	1.60	−0.20	—	—	—	90, 20, 90	
MaCld-Im [a]								
Heme 1	−5.70	−4.70	−4.70	−0.33	0.85	−0.52	10, 0, 0	
Heme 2	−6.40	−5.40	−5.30	−0.33	0.85	−0.52	110, 0, 0	42
His/Im	−5.10	−5.20	−6.00	−0.90	0.38	0.32	40, 0, 0	
MaCld-N_3^- [a]								
Heme 1	−5.80	−5.00	−5.40	−0.33	0.85	−0.52	45, 0, 0	
Heme 2	−6.30	−5.00	−5.40	−0.33	0.85	−0.52	−45, 0, 0	42
His/Im	−4.80	−5.70	−5.30	−0.80	0.12	0.68	90, 0, 0	

α, β, and γ are the Euler angles (in degrees) applied to the ***A*** and ***Q*** tensors frames for each nucleus. Errors on ***A*** values: ±0.05 MHz; errors on *Q* values: ±0.05 MHz; errors on Euler angles: ±10 deg. Im = imidazole, N_3^- = azide. [a] The errors on the literature values are reported in the original paper.[42]

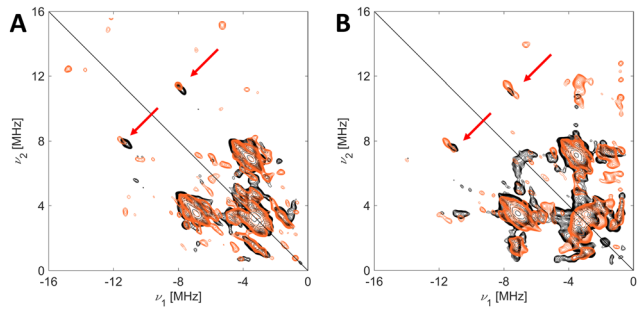

Fig. 6 X-band HYSCORE spectra ((−,+) quadrant) of 1 mM wild-type *C*Cld (black) or CCld R127A (orange) in presence of 500 mM of $^{14}NO_2^-$, taken at the observer position corresponding to $g = g_y(2)$ (A) and $g = g_y(1)$ (B). Only the spectra recorded at τ = 208 ns are displayed. The red arrows indicate the peaks attributed to the strongly coordinated ^{14}N from nitrite.

(Table 1),[22] accounts for about 60% of the total spectral signal, being therefore in excess compared to LS1. Interestingly, in the ^{14}N-HYSCORE of the R127A variant recorded at the field positions $g_y(1)$ and $g = g_y(2^*)$ (Fig. 6), the peaks that we assigned to the strongly coordinated nitrite ^{14}N are clearly visible. This evidence provides a further confirmation that the peaks are indeed associated with this binding mode. Indeed, if they belonged to the *O*-nitrito mode, their intensity would have significantly decreased, considering the smaller contribution of LS1 in the CW-EPR spectrum of the R127 mutant. Note that the relative EPR intensity of LS1–3 also changes with pH for wild-type *C*Cld,[22] but the changes are weaker than in the R127A variant, making the latter variant better suited to prove the relation between binding mode and HYSCORE features. R127 is known to be H-bonded to Q74 in wild-type *C*Cld[22]

Nitrite-binding in chlorite dismutases *versus* myoglobin

The above analysis shows that while for the nitrite complexes of Mb (LS5) and *Ma*Cld (LS4), the *O*-nitrito ligation form is the sole observed binding mode, for *C*Cld also the *N*-nitro ligation (LS2/LS3) is possible besides the dominant *O*-nitrito form (LS1). The principal *g* values of the *O*-nitrito complexes LS4 and LS5 are nearly identical, while those of LS1 differ considerably (Table 1). This is surprising given that the heme-pocket structure of Mb and *Ma*Cld differ considerably, while *Ma*Cld and *C*Cld belong to the same protein family. The crystallographic structure of Mb and *C*Cld in complex with nitrite (Fig. S17) reveals a different orientation of the imidazole residue of the proximal histidine with respect to the heme plane for the two proteins. While in Mb the imidazole plane is oriented along one of the N_{heme}–Fe–N_{heme} directions, it is ~40°–45° turned for *C*Cld. The latter arrangement of the proximal histidine is also found for *Ma*Cld in complex with azide and thiocyanate.[42] Interestingly, also the orientation of the nitrite ligand *versus* the heme ligand is markedly different in the *O*-nitrito complex of *C*Cld compared to Mb, but since no XRD structure of the nitrite complex of *Ma*Cld exists, it is unclear whether this has an influence on the principal *g* values. While in Mb the distal His (His64, Fig. 1B) stabilizes ligand binding, this role is taken up by the distal arginine in chlorite dismutases (Arg127 in *C*Cld, Fig. 1C, and Arg183 in *Ma*Cld). The observation that the H64 V mutation induces a change in the nitrite ligation mode in Mb from *O*-nitrito to *N*-nitro (Fig. 1A and B) shows that the nature of this distal residue is essential to governing the binding mode.[19–21] This is also evident from the nitrite complex formed by the *C*Cld R127A variant, in which the absence of Arg127 promotes the formation of LS2*, associated with the *N*-nitro binding mode, over LS1 (Table 1). In any case, a different ligand-stabilizing residue does not necessarily lead to large differences in the principal *g* values for a specific ligation mode (see *O*-nitrito-forms LS4 and LS5, Table 1). The presence of an H-bonding partner is also not an essential condition for the occurrence of the *O*-nitrito mode. This is demonstrated by the case of the nitrophorins, where the binding through the *N*-nitro mode is

 This journal is © The Royal Society of Chemistry 2026

Open Access Article. Published on 18 March 2026. Downloaded on 5/4/2026 10:46:35 AM. This article is licensed under a Creative Commons Attribution 3.0 Unported Licence.

observed not only in the wild-type form of NP4,[16] which completely lacks any H-bonding residues in the active-site, but also in the NP4(L130R) variant, where an arginine was introduced in the heme proximity.[62] Similarly, in all the nitrite-NiR enzyme complexes characterized so far, the *N*-nitro is the sole binding mode observed, even though the ligand is further hydrogen-bonded to nearby amino acids.[13,63–65] The reactivity towards nitrite could be another determining factor for the different binding modes which distinguish Mb from *C*Cld. Indeed, while Mb possesses a nitrite-reductase activity, being able to easily switch between Fe(II) and Fe(III) oxidation states,[7] this is obviously not the case for *C*Cld, in which no biological function is associated to the Fe(II) state. To favor a specific binding mode is likely important for those systems which naturally interact with nitrite, while in chlorite dismutases the lack of a specific reactivity towards nitrite might explain why no particular binding mode is preferred. Notably, for the globin domain of GLB-33, which possesses an exquisite *in vitro* NiR activity, two pH-dependent nitrite binding modes were recently proposed by some of us.[27] The $g = g_z$ HYSCORE spectrum of the species assigned to the *N*-nitro mode presented in that work shows no signs of the sharp ridges that we here assess as a fingerprint of the *O*-nitrito mode, which further validates our methodology. Interestingly, for both myoglobin and chlorite dismutases systems, the formation of LS complexes upon nitrite binding was undeniable and we found no indication that a conversion to a silent EPR species may have occurred, in contrast to what some studies on nitrite-binding heme proteins suggest.[28–30]

What could explain the observed difference in the EPR data of the two nitrite-ligated chlorite dismutases studied here? First of all, *C*Cld is a Clade-II chlorite dismutase with dimeric structure, while *Ma*Cld is a pentameric Clade-I chlorite dismutase. In both heme pockets, the only charged amino-acid residue is a fully conserved arginine. Studies on *C*Cld have shown that this Arg residue can take on two conformations: pointing inwards to the heme or outwards into the substrate channel.[46] This arginine flexibility can influence ligand stabilization differently in the two Clades, since the hydrogen bonding network is different for both cases. In Clade-II Clds, H-bonding between Arg127 and Gln74 plays an important role in governing the change between the in and out conformations, while this is not the case for Clade-I Clds, which may explain why only the *O*-nitrito ligation mode was found for *Ma*Cld, in contrast to *C*Cld. This may be related to the different orientations that the arginine residue can adopt in the heme pocket, as a result of the intricate interplay between hydrogen bonding to Gln74 and to water molecules, but also interactions with other nearby amino-acids (see SI for more details, Fig. S18), as well as binding to the nitrite ligand and steric effects. Moreover, the discrepancy between the XRD data (only *O*-nitrito) and EPR (both ligation modes) can originate from the different experimental conditions (crystal for XRD, low temperatures in solution for EPR). Given that all analytical techniques have their boundary conditions, it is important to combine these techniques as much as possible with theoretical models. In the case of *C*Cld, molecular modeling indicated that also the *N*-nitro form can co-exist with the more abundant *O*-nitrito form,[22] corroborating the EPR observation.

Conclusions

From the in-depth ^{14}N HYSCORE analysis of low-spin nitrite complexes of ferric myoglobin and two different chlorite dismutases, it follows that the appearance of specific spectral features in the HYSCORE spectra of these proteins can be used to pinpoint *O*-nitrito ligation even when the interpretation of the corresponding CW-EPR spectra is more ambiguous. This approach is transferable to assign nitrite linkage isomerism in heme proteins and synthetic ferric porphyrin complexes, the latter designed for applications nitrite-related applications such as nitrite reductase mimics for biomedicine and biosensing. While a full HYSCORE analysis may be time-consuming or even not possible, it is demonstrated that it may suffice to only measure the HYSCORE spectrum at the low-field side of the EPR spectrum (observer position $g = g_z$) for an identification of the *O*-nitrito bond. Furthermore, we provide first evidence of the appearance of specific $^{14}NO_2^-$ HYSCORE peaks in case of low-spin nitrite complexes of chlorite dismutase with *N*-nitro coordination. Given the extensive discussions and disagreements in literature about how to interpret the EPR data of nitrite-ligated heme proteins,[18,22,24,27,28] the HYSCORE approach presented here constitutes a useful additional tool to settle these controversies.

Author contributions

I. Serra: investigation, formal analysis, data curation, validation, writing – original draft, writing – review & editing. D. Schmidt: resources, writing – review & editing. P. G. Furtmüller: resources, funding acquisition, supervision, writing – review & editing. P. J. González: resources, writing – review & editing. C. Obinger: resources, funding acquisition, supervision, writing – review & editing. S. Van Doorslaer: conceptualization, supervision, funding acquisition, writing – original draft, writing – review & editing. I. García-Rubio: conceptualization, supervision, formal analysis, funding acquisition, writing – original draft, writing – review & editing.

Conflicts of interest

There are no conflicts to declare.

Abbreviations

Cld	Chlorite dismutase
*C*Cld	Chlorite dismutase from *Cyanothece* sp. PCC7425
CW-EPR	Continuous-wave electron paramagnetic resonance
DFT	Density functional theory

Open Access Article. Published on 18 March 2026. Downloaded on 5/4/2026 10:46:35 AM. This article is licensed under a Creative Commons Attribution 3.0 Unported Licence.

DQ	Double-quantum
ESE	Electron–spin-echo
FTIR	Fourier Transform infrared spectroscopy
HS	High-spin
HYSCORE	Hyperfine sublevel correlation
LS	Low-spin
*Ma*Cld	Chlorite dismutase from *Magnetospirillum* sp.
Mb	Myoglobin
NO_3^-	Nitrate
NO	Nitric oxide
NO_2^-	Nitrite
NiR	Nitrite reductase
NPs	Nitrophorins
RR	Resonance Raman spectroscopy
SQ	Single-quantum
NaNO2	sodium nitrite
TIP	Temperature independent buffer
XRD	X-ray diffraction.

Data availability

Data for this article, including raw EPR and HYSCORE spectra are available at OSF at [https://doi.org/10.20350/digitalCSIC/18127].

Supplementary information (SI): CW- and ESE-detected EPR spectra of nitrite complexes of Mb, *C*Cld and *Ma*Cld; additional HYSCORE comparisons; detailed methodology and results of spectral simulations of all HYSCORE spectra; structural comparisons of the active site of nitrite or azide complexes of Mb, *C*Cld and *Ma*Cld. See DOI: https://doi.org/10.1039/d6dt00171h.

Ref. 66–68 are cited in the SI.

Acknowledgements

The authors would like to acknowledge the use of Servicio General de Apoyo a la Investigación-SAI, Universidad de Zaragoza.

This research was funded by the European Union's Horizon 2020 research and innovation program under the Marie Skłodowska-Curie grant agreement no. 813209 and by the grants no. PID2021-127287NB-I00 from the Spanish Ministry of Science and Innovation and E09_23R from regional government of Aragón. The program Severo Ochoa for Centers of Excellence in R&D (CEX2023-01286-S, funded by MICIU/AEI/10.13039/501100011033) is also acknowledged. The authors thank the University of Antwerp (BOF-SEP funding).

References

1 L. B. Maia and J. J. G. Moura, *Chem. Rev.*, 2014, **114**, 5273–5357.
2 A. W. DeMartino, D. B. Kim-Shapiro, R. P. Patel and M. T. Gladwin, *Br. J. Pharmacol.*, 2019, **176**, 228–245.
3 M. T. Gladwin, A. N. Schechter, D. B. Kim-Shapiro, R. P. Patel, N. Hogg, S. Shiva, R. O. Cannon III, M. Kelm, D. A. Wink, M. Graham Espey, E. H. Oldfield, R. M. Pluta, B. A. Freeman, J. R. Lancaster Jr, M. Feelisch and J. O. Lundberg, *Nat. Chem. Biol.*, 2006, **1**, 308–314.
4 A. R. Butler and M. Feelisch, *Circulation*, 2008, **117**, 2151–2159.
5 S. Shiva, S. Frizzell and M. T. Gladwin, in *Nitric Oxide*, Elsevier, 2010, pp. 605–626.
6 K. Cosby, K. S. Partovi, J. H. Crawford, R. P. Patel, C. D. Reiter, S. Martyr, B. K. Yang, M. A. Waclawiw, G. Zalos, X. Xu, K. T. Huang, H. Shields, D. B. Kim-Shapiro, A. N. Schechter, R. O. Cannon and M. T. Gladwin, *Nat. Med.*, 2003, **9**, 1498–1505.
7 M. T. Gladwin and D. B. Kim-Shapiro, *Blood*, 2008, **112**, 2636–2647.
8 T. C. S. Keller, C. Lechauve, A. S. Keller, G. B. Broseghini-Filho, J. T. Butcher, H. R. Askew Page, A. Islam, Z. Y. Tan, L. J. DeLalio, S. Brooks, P. Sharma, K. Hong, W. Xu, A. S. Padilha, C. A. Ruddiman, A. K. Best, E. Macal, D. B. Kim-Shapiro, G. Christ, Z. Yan, M. M. Cortese-Krott, K. Ricart, R. Patel, T. P. Bender, S. K. Sonkusare, M. J. Weiss, H. Ackerman, L. Columbus and B. E. Isakson, *Nat. Commun.*, 2022, **13**, 6405.
9 T. M. Millar, C. R. Stevens, N. Benjamin, R. Eisenthal, R. Harrison and D. R. Blake, *FEBS Lett.*, 1998, **427**, 225–228.
10 M. L. Brennan, W. Wu, X. Fu, Z. Shen, W. Song, H. Frost, C. Vadseth, L. Narine, E. Lenkiewicz, M. T. Borchers, A. J. Lusis, J. J. Lee, N. A. Lee, H. M. Abu-Soud, H. Ischiropoulos and S. L. Hazen, *J. Biol. Chem.*, 2002, **277**, 17415–17427.
11 J. P. Eiserich, M. Hristova, C. E. Cross, A. D. Jones, B. Freeman, B. Halliwell and A. van der Vliet, *Nature*, 1998, **391**, 393–397.
12 O. Einsle, A. Messerschmidt, P. Stach, G. P. Bourenkov, H. D. Bartunik, R. Huber and P. M. H. Kroneck, *Nature*, 1999, **400**, 476–480.
13 S. Nakano, M. Takahashi, A. Sakamoto, H. Morikawa and K. Katayanagi, *Chem. Biodivers.*, 2012, **9**, 1989–1999.
14 F. A. Walker, *J. Inorg. Biochem.*, 2005, **99**, 216–236.
15 D. E. Champagne, R. H. Nussenzveig and J. M. C. Ribeiro, *J. Biol. Chem.*, 1995, **270**, 8691–8695.
16 C. He, H. Ogata and M. Knipp, *Biochemistry*, 2010, **49**, 5841–5851.
17 L. Tilleman, F. Germani, S. De Henau, S. Helbo, F. Desmet, H. Berghmans, S. Van Doorslaer, D. Hoogewijs, L. Schoofs, B. P. Braeckman, L. Moens, A. Fago and S. Dewilde, *J. Biol. Chem.*, 2015, **290**, 10336–10352.
18 C. He, H. Ogata and W. Lubitz, *Chem. Sci.*, 2016, **7**, 5332–5340.
19 D. M. Copeland, A. S. Soares, A. H. West and G. B. Richter-Addo, *J. Inorg. Biochem.*, 2006, **100**, 1413–1425.
20 J. Yi, M. K. Safo and G. B. Richter-Addo, *Biochemistry*, 2008, **47**, 8247–8249.
21 J. Yi, J. Heinecke, H. Tan, P. C. Ford and G. B. Richter-Addo, *J. Am. Chem. Soc.*, 2009, **131**, 18119–18128.
22 I. Serra, D. Schmidt, V. Pfanzagl, G. Mlynek, S. Hofbauer, K. Djinović-Carugo, P. G. Furtmüller, I. García-Rubio,

 This journal is © The Royal Society of Chemistry 2026

Open Access Article. Published on 18 March 2026. Downloaded on 5/4/2026 10:46:35 AM. This article is licensed under a Creative Commons Attribution 3.0 Unported Licence.

S. Van Doorslaer and C. Obinger, *J. Inorg. Biochem.*, 2022, **227**, 111689.
23 Z. N. Nilsson, B. L. Mandella, K. Sen, D. Kekilli, M. A. Hough, P. Moënne-Loccoz, R. W. Strange and C. R. Andrew, *Inorg. Chem.*, 2017, **56**, 13205–13213.
24 M. Sundararajan and F. Neese, *Inorg. Chem.*, 2015, **54**, 7209–7217.
25 W. Tse, N. Whitmore, M. R. Cheesman and N. J. Watmough, *Biochem. J.*, 2021, **478**, 927–942.
26 A. Ioannou, A. Lambrou, V. Daskalakis and E. Pinakoulaki, *J. Inorg. Biochem.*, 2017, **166**, 49–54.
27 N. Van Brempt, R. Sgammato, Q. Beirinckx, D. Hammerschmid, F. Sobott, S. Dewilde, L. Moens, W. Herrebout, C. Johannessen and S. Van Doorslaer, *Biochim. Biophys. Acta, Proteins Proteomics*, 2023, **1871**, 140913.
28 R. Silaghi-Dumitrescu, D. A. Svistunenko, D. Cioloboc, C. Bischin, F. Scurtu and C. E. Cooper, *Nitric Oxide*, 2014, **42**, 32–39.
29 D. E. Schwab, J. S. Stamler and D. J. Singel, *Inorg. Chem.*, 2010, **49**, 6330–6337.
30 S. Basu, R. Grubina, J. Huang, J. Conradie, Z. Huang, A. Jeffers, A. Jiang, X. He, I. Azarov, R. Seibert, A. Mehta, R. Patel, S. B. King, N. Hogg, A. Ghosh, M. T. Gladwin and D. B. Kim-Shapiro, *Nat. Chem. Biol.*, 2007, **3**, 785–794.
31 J. Yi and G. B. Richter-Addo, *Chem. Commun.*, 2012, **48**, 4172.
32 L. L. Bondoc and R. Timkovich, *J. Biol. Chem.*, 1989, **264**, 6134–6145.
33 A. Lambrou and E. Pinakoulaki, *Phys. Chem. Chem. Phys.*, 2015, **17**, 3841–3849.
34 S. Hofbauer, I. Schaffner, P. G. Furtmüller and C. Obinger, *Biotechnol. J.*, 2014, **9**, 461–473.
35 I. Schaffner, S. Hofbauer, M. Krutzler, K. F. Pirker, P. G. Furtmüller and C. Obinger, *Arch. Biochem. Biophys.*, 2015, **574**, 18–26.
36 S. Hofbauer, V. Pfanzagl, H. Michlits, D. Schmidt, C. Obinger and P. G. Furtmüller, *Biochim. Biophys. Acta, Proteins Proteomics*, 2021, **1869**, 140536.
37 M. Zámocký, S. Hofbauer, I. Schaffner, B. Gasselhuber, A. Nicolussi, M. Soudi, K. F. Pirker, P. G. Furtmüller and C. Obinger, *Arch. Biochem. Biophys.*, 2015, **574**, 108–119.
38 A. Famulari, D. Correddu, G. Di Nardo, G. Gilardi, G. Mitrikas, M. Chiesa and I. García-Rubio, *Molecules*, 2024, **29**, 518.
39 I. García-Rubio, M. Fittipaldi, F. Trandafir and S. Van Doorslaer, *Inorg. Chem.*, 2008, **47**, 11294–11304.
40 I. García-Rubio, M. Braun, I. Gromov, L. Thöny-Meyer and A. Schweiger, *Biophys. J.*, 2007, **92**, 1361–1373.
41 I. García-Rubio, J. I. Martínez, R. Picorel, I. Yruela and P. J. Alonso, *J. Am. Chem. Soc.*, 2003, **125**, 15846–15854.
42 A. De Schutter, H. D. Correia, D. M. Freire, M. G. Rivas, A. Rizzi, T. Santos-Silva, P. J. González and S. Van Doorslaer, *J. Phys. Chem. B*, 2015, **119**, 13859–13869.
43 E. Vinck, S. Van Doorslaer, S. Dewilde, G. Mitrikas, A. Schweiger and L. Moens, *J. Biol. Inorg. Chem.*, 2006, **11**, 467–475.
44 S. Van Doorslaer, *J. Magn. Reson.*, 2017, **280**, 79–88.
45 N. Le Breton, J. J. Wright, A. J. Y. Jones, E. Salvadori, H. R. Bridges, J. Hirst and M. M. Roessler, *J. Am. Chem. Soc.*, 2017, **139**, 16319–16326.
46 D. Schmidt, I. Serra, G. Mlynek, V. Pfanzagl, S. Hofbauer, P. G. Furtmüller, K. Djinović-Carugo, S. Van Doorslaer and C. Obinger, *Biochemistry*, 2021, **60**, 621–634.
47 D. M. Freire, M. G. Rivas, A. M. Dias, A. T. Lopes, C. Costa, T. Santos-Silva, S. Van Doorslaer and P. J. González, *J. Inorg. Biochem.*, 2015, **151**, 1–9.
48 A. Schweiger and G. Jeschke, *Principles of Pulse Electron Paramagnetic Resonance*, Oxford University Press, Oxford, 2001.
49 S. Stoll and A. Schweiger, *J. Magn. Reson.*, 2006, **178**, 42–55.
50 M. Bawn and F. Macmillan, *bioRxiv*, 2018, preprint, DOI: 10.1101/252775.
51 P. L. Hagedoorn, D. C. De Geus and W. R. Hagen, *Eur. J. Biochem.*, 2002, **269**, 4905–4911.
52 A. Schweiger and G. Jeschke, *Principles of Pulse Electron Paramagnetic Resonance*, Oxford University Press, 2001.
53 E. Vinck and S. Van Doorslaer, *Phys. Chem. Chem. Phys.*, 2004, **6**, 5324–5330.
54 S. Van Doorslaer, M. van den Bosch, L. Tilleman and S. Dewilde, *Appl. Magn. Reson.*, 2015, **46**, 421–433.
55 C. P. Scholes, K. M. Falkowski, S. Chen and J. Bank, *J. Am. Chem. Soc.*, 1986, **108**, 1660–1671.
56 C. F. Mulks, C. P. Scholes, L. L. C. Dickinson and A. Lapidot, *J. Am. Chem. Soc.*, 1979, **101**, 1645–1654.
57 R. S. Magliozzo and J. Peisach, *Biochemistry*, 1993, **32**, 8446–8456.
58 A. I. Ioanitescu, S. Van Doorslaer, S. Dewilde, B. Endeward and L. Moens, *Mol. Phys.*, 2007, **105**, 2073–2086.
59 D. Goldfarb and S. Stoll, *EPR Spectroscopy: Fundamentals and Methods*, John Wiley & Sons Ltd, 2018.
60 R. Ikeda, M. Mikami, D. Nakamura and M. Kubo, *J. Magn. Reson.*, 1969, **1**, 211–220.
61 J. Kubišta, D. A. Kolářová, V. Shestivska, K. Sovová and P. Španěl, *Appl. Magn. Reson.*, 2020, **51**, 449–460.
62 C. He, H. Ogata and M. Knipp, *Chem. Biodivers.*, 2012, **9**, 1761–1775.
63 P. A. Williams, V. Fulop, E. F. Garman, N. F. W. Saunders, S. J. Ferguson and J. Hajdu, *Nature*, 1997, **389**, 406–412.
64 O. Einsle, A. Messerschmidt, R. Huber, P. M. H. Kroneck and F. Neese, *J. Am. Chem. Soc.*, 2002, **124**, 11737–11745.
65 K. M. Polyakov, K. M. Boyko, T. V. Tikhonova, A. Slutsky, A. N. Antipov, R. A. Zvyagilskaya, A. N. Popov, G. P. Bourenkov, V. S. Lamzin and V. O. Popov, *J. Mol. Biol.*, 2009, **389**, 846–862.
66 A. J. Hoff, A. De Groot, S. A. Dikanov, A. V. Astashkin and Y. D. Tsvetkov, *Chem. Phys. Lett.*, 1985, **118**, 40–47.
67 S. Stoll and A. Schweiger, *J. Magn. Reson.*, 2006, **178**, 42–55.
68 H. L. Flanagan and D. J. Singel, *J. Chem. Phys.*, 1987, **87**, 5606–5616.